ARCHIVES OF ELECTRICAL ENGINEERING VOL. 62(1), pp. 43-54 (2013)

DOI 10.2478/aee-2013-0004

Calculation and analysis of the loss and heat on damper bars in large tubular hydro-generator

YONG LIAO[1], ZHEN-NAN FAN[1], LI HAN[1], LI-DAN XIE[2]

[1] *The State Key Laboratory of Equipment and System Security of Power Transmission and Distribution & New Technology, Electrical Engineering College of Chongqing University Chongqing, 400030, China*

[2]*Guodian Nanjing Automation Co. Ltd., Nanjing, 210003, China*
e-mail: fanzhennan@ 126.com

(Received: 05.08.2012, revised: 31.08.2012)

Abstract: In order to research the losses and heat of damper bars thoroughly, a multi-slice moving electromagnetic field-circuit coupling FE model of tubular hydro-generator and a 3D temperature field FE model of the rotor are built respectively. The factors such as rotor motion and non-linearity of the time-varying electromagnetic field, the stator slots skew, the anisotropic heat conduction of the rotor core lamination and different heat dissipation conditions on the windward and lee side of the poles are considered. Furthermore, according to the different operating conditions, different rotor structures and materials, compositive calculations about the losses and temperatures of the damper bars of a 36 MW generator are carried out, and the data are compared with the test. The results show that the computation precision is satisfied and the generator design is reasonable.

Key words: loss and heat, damper bars, tubular hydro-generator, electromagnetic field and temperature field

1. Introduction

Damper winding is one of the key components of hydro-generator and plays an important role for the safety and stability of generator and power system. The tubular hydro-generator is a good type of hydro-generator which is suitable for exploiting and utilizing the hydraulic resources with low water head and large flowrate. Compared with the axial flowing hydro-generator with the same capability, tubular hydro-generator can economize the project investment 10-25% and increase 3-5% of the power every year, it has then been applied widely at the hydropower stations whose water head is lower than 20 m [1]. However, the electromagnetic and cooling designs of the tubular hydro-generators are more difficult because of its limited inner space and then the more possibility of over heat. In recent years, heavy broken-down failures of damper bars in some large tubular hydro-generators operating at different power stations occurred due to the high temperature at the rated load [2]. To improve the generator design and avoid these serious failures, the amount and distribution of losses and

temperatures within the rotor of the tubular hydro-generators need to be computed more accurately.

Copper losses of field winding and damper bars, as well as iron core losses of rotor lamination, exist within the rotor. For the complex rotor structure of hydro-generator, all of these losses are difficult to compute accurately except the loss of field winding. When the movement of rotor is considered, the heat dissipation condition of the rotor components are more difficult to confirm precisely. Though FE method has been widely used in the temperature field calculation of generators [3-6], the studies in the available literature refers to FE calculation of damper bars losses and temperatures in large tubular hydro-generators are scarce.

In the study of analyze the currents and losses and heat of rotor and damper bar, the reference [7, 8] use a permeance model with Fourier expansion approach to predict the damper winding currents. And an analytical algorithm based on equivalent network is adopted in reference [9] to analyze the damper winding currents and losses when the generator is operated at rated and no-load conditions. In reference [10], a combined numerical and analytical method for the computation of unbalanced magnetic pulls, damper bar currents and losses of laminated low speed hydro-generators in eccentricity conditions under no-load is proposed. And the rotor temperature distribution of hydro-generator is calculated in fluent and temperature field method in reference [11].

In order to research the losses and heat thoroughly and avoid the broken-down failure of damper bars in large tubular hydro-generators, a multi-slice moving electromagnetic field-circuit coupling FE model and a 3D temperature field FE model are established respectively in this paper. The important factors, such as rotor motion and non-linearity of the time-varying electromagnetic field, the stator slots skew, the anisotropic heat conduction of the rotor core lamination and different heat dissipation conditions on the windward and lee side of the poles, are considered. Furthermore, according to the different operating conditions, different rotor structures and materials, compositive calculations about the losses and temperatures of the damper bars of a 36 MW tubular hydro-generator at *Tongzihao* power station are carried out. The design data, which are listed in Table 1, are compared with other large tubular hydro-generators at *Linjintan* and *Feilaixia* power stations. And the results are compared with the test.

2. Calculation models

2.1. Boundary value problem of moving electromagnetic field

According to the periodicity of magnetic field, the area of a pair of poles is chosen as the electromagnetic field calculation region. And along the axial z, the generator is divided into 12 slices, as shown in Figure 1.

Considering the saturation of iron core, the governing equation of nonlinear time-varying electro-magnetic moving field is [12]:

$$\nabla \times (\nu \nabla \times \mathbf{A}) + \sigma \left[\frac{\partial \mathbf{A}}{\partial t} - \mathbf{V} \times (\nabla \times \mathbf{A}) \right] = \mathbf{J_S}, \tag{1}$$

where **A** is vector magnetic potential, $\mathbf{J_s}$ is source current density, v is reluctivity, **V** is velocity and σ is conductivity.

In the multi-slice moving electromagnetic field model, for each slice, the current density and vector magnetic potential have only the axial z components, and the speed has only the axial x component. By coulomb norm $\nabla \cdot \mathbf{A} = 0$ and the boundary condition of the problem region, the 2D boundary value problem of nonlinear time-varying moving electromagnetic field for the generator is then obtained:

$$\begin{cases} \dfrac{\partial}{\partial x}(\nu \dfrac{\partial A_{slz}}{\partial x}) + \dfrac{\partial}{\partial y}(\nu \dfrac{\partial A_{slz}}{\partial y}) = -J_{slz} + \sigma \dfrac{\partial A_{slz}}{\partial t} + V_x \sigma \dfrac{\partial A_{slz}}{\partial x} \\ A_{slz}\big|_{arc\_in} = A_{slz}\big|_{arc\_out} = 0 \\ A_{slz}\big|_{cyclic\_boundary\_start} = A_{slz}\big|_{cyclic\_boundary\_end} \end{cases} \tag{2}$$

Where V_x is the axial x component of velocity, J_{slz} is the axial z component of source current density; A_{slz} is the axial z component of vector magnetic potential.

Table 1. The basic data of the generator

	Tongzihao generator	*Linjintan* generator	*Feilaixia* generator
Rated power (MW)	36	30	35
Rated voltage (kV)	10.5	10.5	10.5
Rated current (A)	2 151	1 736	2 144
Power factor	0.92	0.95	0.9
Rated field current (A)	857	943	1 079
Number of magnetic poles	72	76	72
Number of stator slots	324	342	324
Number of damper bars per pole	4	4	3
Slot skewed in stator	0.5	0	0.5
Damper bar condition	Good	Broken	Broken

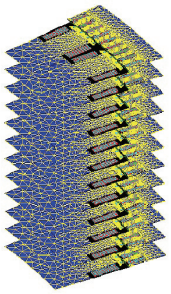

Fig. 1. The problem region and meshes of electromagnetic field

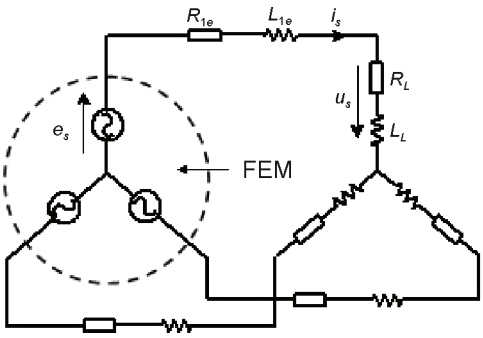

Fig. 2. The coupling circuit of stator

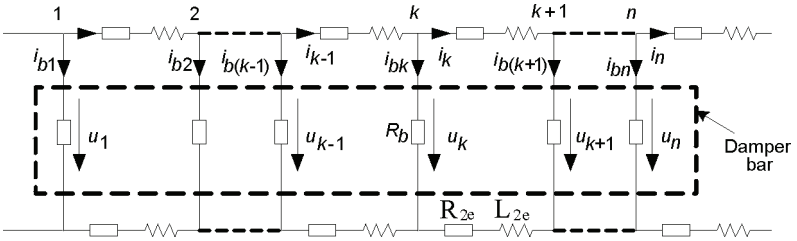

Fig. 3. The coupling circuit of the damper winding

2.2. Coupling circuits

To consider the influence of the end winding of the stator and damper end rings of rotor, the coupling circuit models are established. The external circuit equation and electromagnetic equation should be combined in the calculation [13].

Based on the coupling circuit of stator as shown in Figure 2, the voltage equation of stator circuit is:

$$e_s = u_s + R_{1e} i_s + L_{1e} \frac{di_S}{dt}, \tag{3}$$

where e_s is the inductive EMF of the stator phase winding, u_s and i_s are voltage and current of the stator phase winding respectively, R_{1e} and L_{1e} are the resistance and leakage inductance of the stator end winding respectively.

R_L and L_L are the resistance and inductance of loads respectively. Through change the value of them, different operation conditions of generator can be set.

By the circuit of the damper winding as illustrated in Figure 3, supposing i_{k-1} and i_k are the end ring current of the left and right branches of k^{th} damper bar, the relationship among i_{k-1}, i_k and the current of damper bar i_{bk} can be obtained:

$$i_k - i_{k-1} + i_{bk} = 0. \tag{4}$$

And the voltage equation to describe the relationship between k^{th} and $(k+1)^{\text{th}}$ branches of the damper bars is:

$$u_k - u_{k+1} = 2i_k R_{2e} + 2L_{2e}\frac{di_k}{dt}, \tag{5}$$

where R_{2e} and L_{2e} are the resistance and inductance of the damper end ring, respectively.

According to the periodic condition, the constraint condition of the current and the voltage on the boundary are:

$$i_1 - i_n + i_{b1} = 0, \tag{6}$$

$$u_n - u_1 = 2i_n R_{2e} + 2L_{2e}\frac{di_n}{dt}, \tag{7}$$

where n is the number of damper bars in the problem region.

The stator rotor coupling circuit equation of generator and the electromagnetic equation are combined, the magnetic vector A_{slz} of slices is calculated in time-step finite element method, then the flux density, voltage, current and loss can be got.

2.3. Boundary value problem of rotor 3D temperature field

Because of the symmetric structures of the rotor pole and its ventilation system, the distribution of rotor temperature field is mirror symmetric on the both sides of the rotor shaft middle profile. Therefore, an half axial section of the rotor, which consist of rotor core, damper winding, field winding and its bracket, insulation, et al, are selected as the problem region for the 3D temperature field, and the region includes 25 6256 elements and 13 7260 nodes.

Considered of the anisotropic heat conduction condition of the rotor core, the boundary value problem of 3D steady temperature field can be expressed as follows:

$$\begin{cases} \dfrac{\partial}{\partial x}(\lambda_x \dfrac{\partial T}{\partial x}) + \dfrac{\partial}{\partial y}(\lambda_y \dfrac{\partial T}{\partial y}) + \dfrac{\partial}{\partial z}(\lambda_z \dfrac{\partial T}{\partial z}) = -q_V \\ \lambda \dfrac{\partial T}{\partial n}\Big|_{S_2} = 0 \\ \lambda \dfrac{\partial T}{\partial n}\Big|_{S_3} = -\alpha(T - T_f) \end{cases} \tag{8}$$

where T is temperature, λ_x, λ_y and λ_z are heat conductivity on each direction, q_v is the heat source density which is obtained by losses calculation, S_2 are the rotor middle profile and the interface between rotor core and rim related with the thermal insulation boundary condition, S_3 are the outside surfaces of the rotor related with the heat dissipation boundary condition, α is the heat dissipation coefficient of S_3 and T_f is the environmental air temperature. The problem regions are illustrated in Figure 4.

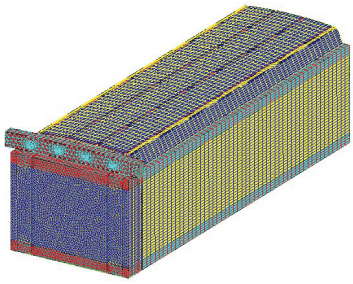

Fig. 4. The problem region and boundary conditions of 3D temperature field

3. Computation results and discussions

Based on the models established above, the compositive computations of the multi-slice moving electromagnetic field-circuit coupling FE model and 3D temperature field FE model of the 36 MW tubular hydro-generator at *Tongzihao* power station are carried out. There are 4 damper bars on each pole shoe. For easy discussion of the computing results, the damper bar on the lee side is numbered 1th and the damper bar on the windward is numbered 4th.

3.1. The influence of operating conditions

Figure 5 gives the electromagnetic field, and the temperature distributions on the no load and symmetric rated load of the generator respectively. Table 2 gives the losses and temperatures of the damper bars of these 2 operating conditions.

Table 2. Losses and temperatures of the damper bars with different operating conditions

Operation condition	Loss (W)					Temperature (°C)	
	P_1	P_2	P_3	P_4	$\sum P$	T_{max}	T_{min}
No load	108	44	44	108	305	99	70
Rated load	635	308	141	70	1154	146	77

where P_1-P_4 and $\sum P$ are the losses of the 1th-4th damper bar and the total losses of the damper bars respectively, T_{max} and T_{min} are the maximal and minimal temperature of the damper bars respectively.

Figure 5 and Table 2 show that the distribution of the magnetic field about the central axis of the pole is symmetric when the generator operates with no load, and the eddy current and loss of the damper bar are then basically symmetrical about the pole center axis. The losses of the 1th and 4th damper bar are roughly equal, the losses of the 2th and 3th damper bar are roughly equal, too. Because of the armature reaction, the distribution of the airgap magnetic field is distorted when the generator operates with rated load.

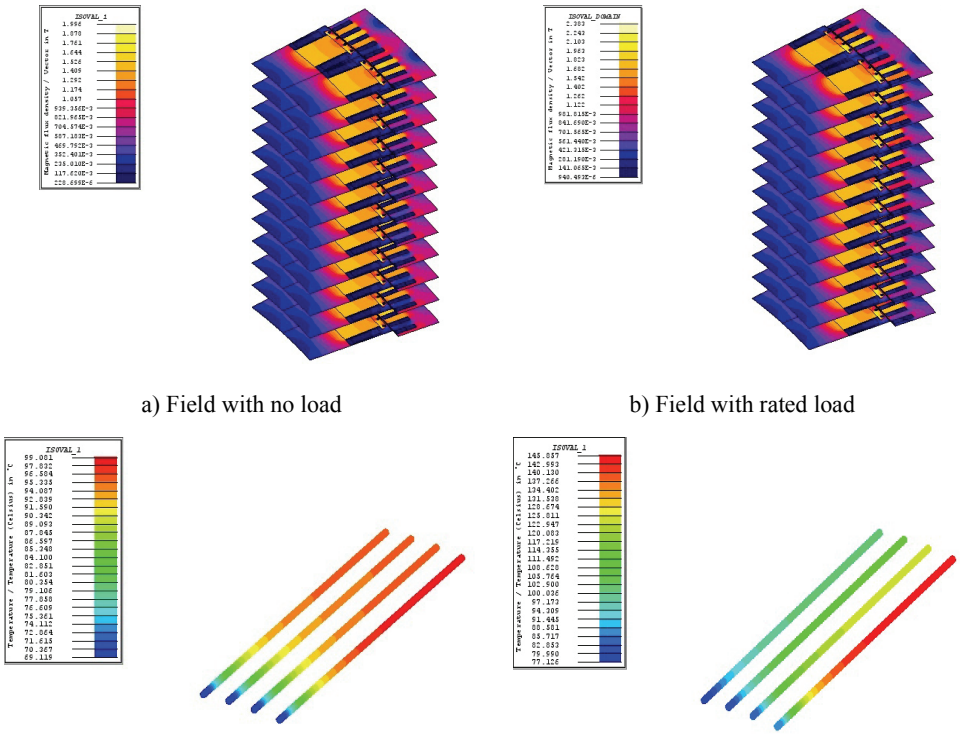

a) Field with no load

b) Field with rated load

c) Bar temperature with no load

d) Bar temperature with rated load

Fig. 5. Electromagnetic field and temperature distributions of damper bars

The magnetic field on the windward is weakened while it is strengthened on the lee side. The symmetry of the eddy current and loss distribution of the damper bars will no longer existed. The eddy current and loss of the 1th damper bar are significantly larger than those of the 4th damper bar. The temperature of the damper bars located near the lee side is higher than that of located near the windward. The maximal temperature occurs at the axis middle of the 1th damper bar and the minimal temperature occurs at the end of the 4th damper bar. The loss and the temperature of the damper bars increase obviously when the operating conditions of the generator change from no load to symmetric rated load. At the symmetric rated load, the maximal temperature is 1.47 times higher than that of no load, that is to say the temperature increases 47°C. The results show that the operating conditions influence the loss and heat of the damper bars obviously. In the following discussions, the operating condition of symmetric rated load will be focused.

3.2. The influence of damper bar pitch

Losses and temperatures of the damper bars for 4 different damper bar pitch with symmetric rated load are listed in the Table 3, in which t_1 is the stator slot pitch and keeps

unchanged, t_2 is the damper bar pitch. The results show that the losses and temperatures of damper bars increase obviously with the decrease of t_2. Because of the uneven airgap of the generator, when t_2 decreases, each damper bar gets closer to the center axis of the pole and larger eddy current is induced. Therefore, the losses and temperatures of the damper bars also increase. When t_2/t_1 decreases from 0.93 to 0.6, the maximal temperature of the damper bar increases from 146°C to 213°C and the temperature rise is 67°C.

Design data t_2/t_1 of the generators at *Tongzihao*, *Linjintan* and *Feilaixia* hydropower stations are 0.93, 0.59 and 0.9 respectively. It is easy to find that the design of *Tongzihao* hydro-generator is more reasonable for avoiding over heat. In the following discussions, keep $t_2/t_1 = 0.93$ constant.

3.3. The influence of damper bar assembling airgap

The air gap between the damper bar and the damper slot is called assembling airgap in this paper and is symbolized as δ_B. Temperatures of the damper bars for 3 different δ_B with symmetric rated load are listed in Table 4.

Because δ_B is very small and has few influence on the electromagnetic field, the losses of the damper bars for different δ_B are basically the same and then not be tabled. On the other hand, with the increase of δ_B, the heat conductivity of the assembling airgap becomes smaller and the temperature of the damper bars becomes higher. To control the temperature rise of the damper bars, it is necessary to limit δ_B. Design data δ_B of the generators at *Tongzihao*, *Linjintan* and *Feilaixia* hydropower stations are 0.15 mm, 0.5 mm and 0.4 mm respectively. The design of *Tongzihao* hydro-generator is more reasonable for avoiding over heat.

3.4. The influence of airgap length

Keeping the stator slot width b_s unchanged and reducing the airgap length δ, more computations are carried out. Losses and temperatures of the damper bars for 3 different δ within symmetric rated load are listed in Table 5.

With the decrease of δ, the airgap flux density and the stator tooth harmonics increase. These factors lead to the increase of the loss and temperature of the damper bars. Design data b_s/δ of the generators at *Tongzihao*, *Linjintan* and *Feilaixia* hydropower stations are 3.4, 3.2 and 2.9 respectively. However, the uneven airgap length is used on *Tongzihao* generator and the equivalent b_s/δ is 2.7 when uniform airgap is referred.

3.5. The influence of damper bar diameter

To discuss the influence of damper bar diameter d_B, losses and temperatures of 3 different d_B with symmetric rated load are listed in Table 6.

With the decrease of d_B, the total losses of the damper bars decrease too. However, the loss density, heat resistance of the assembling airgap and then the temperature of the damper bars increase due to the decrease of d_B. To prevent from the over heat and mechanical vibration of the damper bars, d_B should be enlarged appropriately. Design data d_B of the generators at *Tongzihao*, *Linjintan* and *Feilaixia* hydropower stations are 15 mm, 9.5 mm and 16 mm respectively.

3.6. The influence of damper bar resistivity

To discuss the influence of conductive materials on the losses and temperatures, 3 different damper bar materials are used and their resistivities ρ_B at 120°C are listed in Table 7. The losses and temperatures of the damper bars for 3 different ρ_B with symmetric rated load are listed in Table 8. The results show that the losses and temperatures of the damper bars decrease with the increase of ρ_B.

3.7. The influence of heat dissipation coefficient of field winding

Temperatures of the damper bars for 4 different heat dissipation coefficients of field winding with symmetric rated load are listed in Table 9. The surface heat dissipation coefficients of field winding with the rectangular and septangular cross sections are 72.8 W/m^2 ·°C and 101.1 W/m^2 ·°C respectively. The results show that the field winding with the septangular cross section leads to a lower temperature of damper bars due to its larger surface area of heat dissipation.

Table 3. Losses and temperatures of the damper bars for different pitch

t_2/t_1	Loss (W)					Temperature (°C)	
	P_1	P_2	P_3	P_4	$\sum P$	T_{max}	T_{min}
0.93	635	308	141	70	1154	146	77
0.80	998	615	296	125	2034	181	89
0.70	1003	1021	431	134	2589	191	97
0.60	893	1290	545	152	2853	213	103

Table 4. Temperatures of the damper bars for different δB

δ_B (mm)	T_{max} (°C)	T_{min} (°C)
0	117	82
0.15	146	77
0.25	168	78

Table 5. Losses and temperatures of the damper bars for different airgap

b_s/δ	Loss (W)					Temperature (°C)	
	P_1	P_2	P_3	P_4	$\sum P$	T_{max}	T_{min}
2.5	389	219	99	62	769	136	78
3.4	635	308	141	70	1154	146	77
4.0	813	429	179	79	1500	159	72

Table 6. Losses and temperatures of the damper bars for different dB

d_B (mm)	Loss (W)					Temperature (°C)	
	P_1	P_2	P_3	P_4	$\sum P$	T_{max}	T_{min}
20	698	357	202	100	1357	142	75
15	635	308	141	70	1154	146	77
9.5	490	218	127	85	920	148	79

Table 7. Resistivities for different materials of damper bars

Material	Copper	Alloy	Brass
resistivity ρ_B ($\times 10^{-7}$ Ωm)	0.25	0.4	0.77

Table 8. Losses and temperatures of the damper bars for different ρB

Material	Loss (W)					Temperature (°C)	
	P_1	P_2	P_3	P_4	$\sum P$	T_{max}	T_{min}
Copper	635	308	141	70	1154	146	77
Alloy	623	279	145	75	1122	145	76
Brass	568	233	157	98	1056	141	77

Table 9. Temperatures of the damper bars for different heat dissipation coefficients of field winding

Heat dissipation coefficient (W/m^2°C)	T_{max} (°C)	T_{min} (°C)
101.1	145.9	77.1
91.0	147.9	78.0
80.9	150.4	79.8
72.8	152.6	80.2

Table 10. Temperatures of the damper bars for different rotor core materials

λ_r/λ_a	T_{max} (°C)		T_{min} (°C)	
	Copper bar	Brass bar	Copper bar	Brass bar
55.6/4.0	144.0	140.5	79.8	67.5
51/19.6	145.9	141.6	77.1	68.0
40.6/3.4	154.1	141.9	78.5	67.3
19/4.0	158.8	146.2	78.8	68.9
16/1.95	160.2	147.5	78.9	69.0

3.8. The influence of heat conductivity of iron core

Considering the anisotropic heat conductivity of the rotor core lamination, the radial and axial heat conductivities, λ_r and λ_a, are different. Temperatures of the damper bars for 5 different core materials with symmetric rated load are listed in Table 10. The results show that the better heat conductivity of the rotor core lamination can help for reduces the temperature of damper bars.

3.9. Verification of the results

To verify the correctness of the calculation models in this paper, the temperature test of the field winding is carried out at *Tongzihao* hydropower station. The environmental air temperature is 47.6°C and the average temperature of field winding tested is 110°C with the rated load of the generator. To compare with the test data, more temperatures of the rotor parts, including damper bar, field winding and iron core, are obtained by the compositive calculations of the multi-slice moving electromagnetic field-circuit coupling FE model and 3D anisotropic

steady temperature field FE model. The calculated average temperature of field winding is 106°C and is well agreed with the test dada. The relative error between the calculation and the test is less than 3.6%.

4. Conclusions

Compared with the traditional analytical model and steady magnetic field FE model, The models proposed in this paper are more reasonable and can obtain more accurate results by compositive calculations of the multi-slice moving electromagnetic field-circuit coupling FE model and 3D anisotropic steady temperature field FE model.

The losses and heat distributions of the damper bars in one pole are uneven with the rated load. The loss and temperature of the damper bars near the lee side are higher than that of the windward.

The operating conditions and the structure design of the generator are the main factors which influence the loss and heat of damper bars. The effective methods for preventing from over heat of the damper bars are avoiding over load and asymmetric load of the generator, enlarging the damper bar pitch, increasing the airgap and decreasing assembling airgap of the damper bar, et al.

The designed 36 MW tubular hydro-generator has been operating safely all the times at *Tongzihao* hydropower station since July 2003. The good operating experience, as well as the good agreement between the computation and the test, shows that the computing models and design results of this paper are correct.

Acknowledgements
This work was sponsored by the Fundamental Research for the Central Universities Project No.CDJXS11151152.

References

[1] Chao-Yang Li, *The Application of Bulb-type Hydro-Generator Set at Low Head Hydropower Station.* Developing 9: 145-146 (2006).
[2] Jing-Bin Guo, *Analysis of Damaged Damping Winding and Magnetic Pole in Bulb Type Generator.* Chinese Power 34(7): 63-67 (2001).
[3] Armor A.F., Chari M.V.K., *Heat Flow in the Stator Core of Large Turbine Generators by the Method of Three-Dimensional Finite Elements.* IEEE Trans. on PAS. 95(5): 1648-1668 (1976).
[4] Armor A.F., *Transient, Three-Dimensional, Finite-Element Analysis of Heat Flow in Turbine-Generator Rotors*. IEEE Trans. on PAS. 99(3): 934-946 (1980).
[5] Khan G.K.M., Buckley G.W., Bennett R.B., Brooks N., *An Integrated Approach for the Calculation of Losses and Temperatures in the End-Region of Large Turbine Generators.* IEEE Trans. on Energy Conversion 5(1): 183-194 (1990).
[6] Karmaker H.C., *Broken Damper Bar Detection Studies Using Flux Probe Measurements and Time-Stepping Finite Element Analysis for Salient-Pole Synchronous Machines.* Symposium on Diagnostics for Electric Machines, Power Electronics and Drives, pp. 193-197 (2003).

[7] Knight A.M., Karmaker H., Weeber K., *Prediction of damper winding currents and force harmonic components in large synchronous machines.* Proc.15th ICEM, p. 35 (2002).
[8] Knight A.M., Karmaker H., Weeber K., *Use of a permeance model to predict force harmonic components and damper winding effects in salient pole synchronous machines.* IEEE Trans. on Energy Conversion 17(4): 478-484 (2002).
[9] Traxler-Samek G., Lugand S., Schwery A., *Add loss in the Damper Winding of Large Hydrogenerator at Open-Circuit and Load Conditions.* IEEE Trans. on Industrial Electronics 57(1): 154-160 (2010).
[10] Keller S., Xuan M.Tu., Simond J.-J., Chwery A., *Large low-speed hydro-generator-unbalanced magnetic pulls and additional damper losses in eccentricity conditions.* IET Electr. Power Appl. 21(5): 657-664 (2007).
[11] Xia Hai-xia, Yao Ying-ying, Ni Guang-zheng, *Analysis of ventilation fluid field and rotor temperature field of a generator*. Electric Machines and Control 11(5): 472-476 (2007).
[12] Min-Qiang Hu, Xue-Liang Huang, *Numerical Computation Method and its Application of Electric Machine Performance.* Nanjing: Southeast University Press (2003).
[13] Piriou F., Razek A., *Finite element analysis in electromagnetic systemsaccounting for electric circuits*. IEEE Trans on Magnetics 29(2): 1669-1675 (1993).